Astron. Astrophys. 335, 329–340 (1998)

ASTRONOMY AND ASTROPHYSICS

Random driven fast waves in coronal loops

I. Without coupling to Alfvén waves

A. De Groof, W.J. Tirry*, and M. Goossens

Centre for Plasma Astrophysics, K.U. Leuven, Celestijnenlaan 200 B, B-3001 Heverlee, Belgium

Received 1 December 1997 / Accepted 24 March 1998

Abstract. In this paper we study the time evolution of fast MHD waves in a coronal loop driven by footpoint motions in linear ideal MHD. We restrict the analysis to footpoint motions polarized normal to the magnetic flux surfaces such that the fast waves are driven directly. By supposing the azimuthal wave number k_y to be zero, the fast waves are decoupled from the Alfvén waves.

As a first step to real stochastic driving, we consider the loop to be driven by a train of identical pulses with random time intervals in between. The solution is written as a superposition of eigenmodes whose excitation is determined by the time dependence of the footpoint motion through a convolution and by the spatial dependence of the footpoint motion through a scalar product.

An important result from the simulations is that the amount of kinetic energy associated with the body modes is much larger than the amount corresponding to the leaky modes. This means that most of the input energy is stored within the loop. For $k_y \neq 0$, body modes can resonantly couple to Alfvén waves at certain magnetic surfaces and hence the energy of the body modes can then be dissipated around the resonant magnetic surfaces.

Using a gamma distribution for the time intervals between the successive pulses, we analytically derive a relation between the mean value of the kinetic energy contribution of each eigenmode, the eigenfrequency, the number of pulses and the width of the pulses. The larger the variance of the distribution, the less the power spectrum reveals fine structure, peaks around certain preferred frequencies. The analytical results confirm the output from the numerical simulations.

Key words: MHD – Sun: corona – Sun: magnetic fields-waves – waves

1. Introduction

Since Skylab it is known that the extremely hot corona (roughly 3×10^6 K) is a complex medium, structured by the magnetic field in myriads of dynamic coronal loops. Moreover the X-ray images show that these magnetic loops have the largest heating requirements.

The high conductivity and the relatively high mass density of the photospheric plasma provide an effective photospheric anchoring of the coronal magnetic field lines. The photospheric footpoints of the magnetic field lines are forced to follow the convective motions. If these footpoint motions are 'slow' (in comparison with the Alfvénic transit time along the loop), the coronal flux tubes are slowly twisted and braided. The magnetic stresses, which are built up that way, and the small length scales in between fieldlines of different polarity, lead to magnetic reconnection and hence to a conversion of magnetic energy into heat (Parker 1972).

In contrast, footpoint motions which are 'fast' in comparison with the Alfvénic transit time, generate magnetosonic waves and Alfvén waves. Due to the steep density gradients at the photospheric edges these MHD waves are reflected back and forth along the length of the loop. The loop is then expected to act as a leaking, resonant cavity for MHD waves (Hollweg 1984), in which dissipation is enhanced by means of turbulence (Gomez 1990), resonant absorption (Goossens 1991) and/or phase mixing (Heyvaerts & Priest 1983).

Plasma heating by resonant absorption of Alfvén waves hinges on the existence of a continuous part of the Alfvén spectrum in linear ideal MHD. Tataronis & Grossmann (1975) were the first to give a basic theory on plasma heating by these Alfvén continuum waves. Chen & Hasegawa (1974) and Kappraff & Tataronis (1977) elaborated on Alfvén continuum waves as effective heaters of fusion plasmas. Shortly after, Ionson (1978) suggested that resonant absorption might effectively heat the solar corona.

A lot of work, both analytically and numerically, was done on sideways excitation of these resonant Alfvén waves where a wave impinges laterally on the loop (Poedts et al. 1989; Poedts & Kerner 1992; Steinolfson & Davila 1993; Ofman & Davila 1995, 1996; Wright & Rickard 1995). When a loop is perturbed by a broad band spectrum on its side surface, it will respond at a discrete set of frequencies of fast waves which may resonantly excite Alfvén waves in turn. Hence the plasma-driver coupling was found to be very efficient due to the effect of the present quasi-modes.

Send offprint requests to: A. De Groof

* Research Assistant of the F.W.O.-Vlaanderen

However it is important to see that sideways excitation by an externally impinging fast wave can only yield a minor contribution to the heating of a coronal loop by resonant absorption. Due to the enhanced density the interior Alfvén speed must be smaller than the exterior Alfvén speed. Therefore only fast waves which are exponentially decaying on their way to the loop can resonantly excite Alfvén waves inside the loop. This suggests that fast waves originating from within the loop must be the prime contribution. Such fast wave can be excited by e.g. a reconnection event inside the loop or by the photospheric motions of the footpoints of the magnetic field lines.

Recently, more attention is paid to the fact that coronal loops are finite and bounded by the photospheric plasma. Strauss & Lawson (1989) considered MHD simulations of resonant absorption in an incompressible cylindrical plasma that is excited at his footpoints. This is one of the first papers in which the consequences of line-tying is discussed. Later on, it was shown analytically that line-tying completely changes the character of the basic MHD waves occuring in a coronal loop as compared to those in a periodic system. MHD waves of mixed nature occur: the waves consist of large amplitude Alfvén components in the corona and fast components with a small but rapidly varying amplitude in the photospheric boundary layers (Goedbloed & Halberstadt 1994). The subsequent paper by Halberstadt & Goedbloed (1995) discusses the coupling in the stationary state between fast and Alfvén waves in a cylinder with helical magnetic field for which the footpoint excitation has both an Alfvén wave polarization and a fast wave polarization.

Berghmans & De Bruyne (1995) and Ruderman et al. (1997) studied the direct excitation of resonant Alfvén waves by azimuthally polarized footpoint motions in ideal and dissipative MHD respectively. Berghmans & Tirry (1997) and Tirry & Berghmans (1997) showed how the results can be drastically changed when the coupling to fast waves is taken into account. On the other hand Berghmans, De Bruyne & Goossens (1996) investigated the temporal behaviour of the sausage fast wave excited by radially polarized footpoint motions, whereas Tirry, Berghmans & Goossens (1997) revealed the importance of the quasi-mode in this indirect driving of resonant Alfvén waves.

So far, most of the analyses focussed on a periodic driving or a driving by one pulse. In the present paper we want to figure out how the results alter for randomly driven footpoint motions. We start to consider a loop that is driven by a train of pulses with random time-intervals in between and to look at the behaviour of the fast waves within the loop without coupling to Alfvén waves.

The paper is organized as follows. In the next section, the physical model with the relevant equations and boundary conditions is discussed. In Sect. 3 we repeat the important steps in the derivation of the analytical solution, which describes the temporal behaviour of the excited MHD waves, as given by Tirry, Berghmans & Goossens (1997). The solution is written as a superposition of eigenmodes. In Sect. 4 we classify these eigenmodes as leaky or body modes, whereas in Sect. 5 we look how the input energy is spread over the different modes. Sect. 6 is devoted to obtain analytically a relationship between the mean value of the kinetic energy contribution of each eigenmode and the eigenfrequency. In Sect. 7 the results are discussed. Finally in Sect. 8 we give a summary.

2. Physical model

A coronal loop is modelled as a static, straight, gravitationless plasma slab with thickness b, obeying the standard set of ideal linearized MHD equations. In the Cartesian coordinate system we use, the x-coordinate corresponds to the radial direction (the direction of the inhomogeneity in the equilibrium), the y-coordinate is the (ignorable) azimuthal coordinate and the z-coordinate represents the direction along the loop.

At $z = 0$ we impose a given footpoint motion whereas at $z = L$ we assume the loop to be line-tied. This can be done without any loss of generality because of the principle of superposition for solutions of linear equations. The boundary planes model the sharp transition from the corona to the photosphere (i.e. transition region, chromosphere and photosphere). We refer to these boundary planes as the 'photospheric edges' of the loop and we implicitly assume that a disturbance initiated in the photosphere indeed reaches the corona. In the radial direction we assume for mathematical tractability rigid wall conditions at $x = 0$ and $x = b$. The two boundaries $x = 0$ and $x = b$ correspond to the interior of the loop and the exterior coronal environment respectively.

The plasma is permeated by a uniform magnetic field ($\mathbf{B_0} = B_0\mathbf{e_z}$) and has a uniform pressure p_0 which we neglect in comparison with the magnetic pressure ('zero-beta-approximation'). The inhomogeneity of the plasma is introduced by a continuously varying density

$$\rho_0(x) = \rho_A + \rho_B \cos(\frac{\pi}{b}x) \quad \text{with} \quad \rho_B < \rho_A, \tag{1}$$

which models the higher density inside the loop.

The plasma is being shaken by small-amplitude perturbations at the footpoints of the magnetic field lines on the $z = 0$ plane. As long as non-linear and non-ideal effects are negligible we can follow the temporal evolution of the excited MHD waves inside the loop by solving the linear ideal MHD equations. These equations reduce for a pressureless plasma to

$$\{\frac{1}{v_A^2}\frac{\partial^2}{\partial t^2} - \frac{\partial^2}{\partial z^2} - \frac{\partial^2}{\partial x^2}\}\xi_x = \frac{\partial^2 \xi_y}{\partial y \partial x}, \tag{2}$$

$$\{\frac{1}{v_A^2}\frac{\partial^2}{\partial t^2} - \frac{\partial^2}{\partial z^2} - \frac{\partial^2}{\partial y^2}\}\xi_y = \frac{\partial^2 \xi_x}{\partial y \partial x}, \tag{3}$$

where $\boldsymbol{\xi}$ is the Lagrangian displacement and the Alfvén speed v_A is given by

$$v_A(x) = \sqrt{\frac{B_0^2}{\rho_0(x)}}.$$

This coupled system of partial differential equations in ξ_x and ξ_y describes the coupled fast-Alfvén waves. Slow waves are absent ($\xi_z = 0$) because the plasma pressure is neglected.

Since the equilibrium quantities are constant in the y-coordinate which runs over an infinite interval, we can Fourier

analyse with respect to y. For the Fourier component corresponding to wave number k_y, the time evolution and the spatial variation in x and z are described by

$$\{\frac{1}{v_A^2}\frac{\partial^2}{\partial t^2}-\frac{\partial^2}{\partial z^2}-\frac{\partial^2}{\partial x^2}\}\xi_x \;=\; ik_y\frac{\partial \xi_y}{\partial x}, \tag{4}$$

$$\{\frac{1}{v_A^2}\frac{\partial^2}{\partial t^2}-\frac{\partial^2}{\partial z^2}+k_y^2\}\xi_y \;=\; ik_y\frac{\partial \xi_x}{\partial x}. \tag{5}$$

For $k_y = 0$ these equations are decoupled: Eq. (4) describes the evolution of the fast waves, whereas Eq. (5) governs the behaviour of the Alfvén waves. In this paper we shall focus on y-independent fast waves excited by stochastic radially polarized footpoint motions. For the rest of the paper, length, speed, magnetic field strength and density are non-dimensionalized with respect to b, $v_A(0)$, B_0 and $\rho(0)$ respectively.

3. Mathematical approach

At first we represent the footpoint motions by inhomogeneous boundary conditions for Eqs. (4) and (5) at the $z = 0$ and the $z = L$ boundary planes:

$$\begin{aligned}
\xi_x(x,z=0,t) &= R(x)T(t),\\
\xi_x(x,z=L,t) &= 0,\\
\xi_y(x,z=0,t) &= 0,\\
\xi_y(x,z=L,t) &= 0.
\end{aligned} \tag{6}$$

We have assumed for mathematical simplicity that the dependencies on x and t of the footpoint motions are separable. In order to avoid complications with initial conditions we assume in addition that at $t = 0$, ξ_x, ξ_y and both their time derivatives are zero and as a consequence:

$$T(t=0)=\frac{\partial T(t=0)}{\partial t}=0.$$

Apart from these restrictions the functions $R(x)$ and $T(t)$ can be chosen completely arbitrarily.

A convenient way to solve the coupled partial differential Eqs. (4-5) is to get rid of as many derivatives as possible. First of all we can remove the z-derivatives. By introducing the function

$$\chi(x,z,t)=\xi_x(x,z,t)-(1-\frac{z}{L})R(x)T(t),$$

we include the footpoint motions as driving terms in the equations. The boundary conditions then become homogeneous which allows us to expand $\chi(x,z,t)$, $i\xi_y(x,z,t)$ and $(1-z/L)$ in a series of sines.

With the use of these sine transforms the coupled partial differential Eqs. (4) and (5) are replaced by an infinite set of coupled partial differential equations for $X^{(n)}$ and $Y^{(n)}$, the 'nth' coefficients in the series of sines of χ and $i\xi_y$ respectively. There is no coupling between different n-modes.

By taking the Laplace transform of these coupled equations, we also remove the time-derivative in the equations. We then are left with two coupled equations for each n :

$$\{A[n]-\omega^2\}\begin{bmatrix}\hat{X}^{(n)}\\ \hat{Y}^{(n)}\end{bmatrix}=B[n] \tag{7}$$

where $A[n]$ only contains derivatives with respect to x and $B[n]$ is dependent on $T(t)$ and $R(x)$. Eq. (7) can be solved by inversion of the operator $A[n]-\omega^2$. Formally this is not a problem, because $A[n]$ corresponds to the ideal MHD force operator which is Hermitian with respect to the following scalar product

$$<\xi_{\mathbf{1}}|\xi_{\mathbf{2}}>=\int_0^b \xi_{\mathbf{1}}\cdot\xi_{\mathbf{2}}^*\,\rho\,dx. \tag{8}$$

It is well known that the eigenfunctions form a complete set so that the solution to Eq. (7) can be written as a spectral representation:

$$\begin{aligned}
\begin{bmatrix}\hat{X}^{(n)}\\ \hat{Y}^{(n)}\end{bmatrix} &= \sum_k \frac{1}{\omega_k^{(n)2}-\omega^2}|\psi_k^n><\psi_k^n|B[n]>\\
&+ \int \frac{1}{\sigma^{(n)2}-\omega^2}|\psi_\sigma^n><\psi_\sigma^n|B[n]>d\sigma,
\end{aligned}$$

with orthonormal discrete and continuum eigenfunctions satisfying the orthonormal relationships :

$$\begin{aligned}
<\psi_k^n|\psi_l^n> &= \delta_{kl},\\
<\psi_\sigma^n|\psi_\gamma^n> &= \delta(\sigma-\gamma),\\
<\psi_k^n|\psi_\sigma^n> &= 0.
\end{aligned}$$

The boundary conditions in the x-direction and the form of the Eqs. (4-5) suggest that the first component and the second component of the eigenfunction can be expanded in series of sines and cosines respectively.

By inverting the Laplace transformation, recalling the definition of χ and the sine transformations, we obtain the following solution for ξ_x and ξ_y as function of x, z and t:

$$\begin{aligned}
&\xi_x(x,z,t)=\frac{2}{L}\sum_{n=1}^{\infty}\\
&\sum_{m=1}^{N}\left\{\frac{n\pi}{L}\sum_{k=1}^{2N+1}\mathcal{R}_k^nT_k^n(t)\alpha_{mk}^n\right\}\sin(\frac{m\pi x}{b})\sin(\frac{n\pi}{L}z)\\
&+R(x)T(t)\left\{1-\frac{z}{L}-\frac{2}{L}\sum_{n=1}^{\infty}\frac{L}{n\pi}\sin(\frac{n\pi}{L}z)\right\},
\end{aligned} \tag{9}$$

$$\begin{aligned}
&i\xi_y(x,z,t)=\\
&\frac{2}{L}\sum_{n=1}^{\infty}\frac{n\pi}{L}\{\sum_{k=1}^{2N+1}\mathcal{R}_k^nT_k^n(t)\frac{\beta_{0k}^n}{2}\\
&+\sum_{m=1}^{N}\left(\sum_{k=1}^{2N+1}\mathcal{R}_k^nT_k^n(t)\beta_{mk}^n\right)\cos(\frac{m\pi x}{b})\}\sin(\frac{n\pi}{L}z).
\end{aligned} \tag{10}$$

In these equations, T_k^n is the time convolution:

$$T_k^n\equiv\frac{1}{\omega_k^{(n)}}\int_0^t\sin(\omega_k^{(n)}(t-\tau))T(\tau)d\tau$$

and $\mathcal{R}_k^n$ is the scalar product of $R(x)$ and the eigenfunction $|\psi_k^n>$ without weight function:

$$\mathcal{R}_k^n\equiv\int_0^b R(x)|\psi_k^n(x)>_1 dx.$$

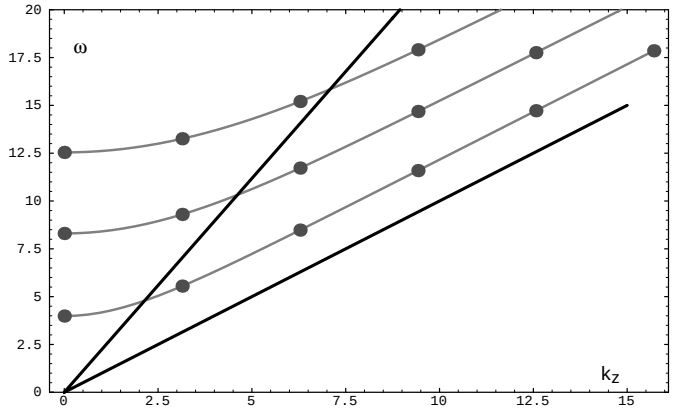

Fig. 1. The eigenfrequencies of the first three fast eigenmodes (gray lines) together withe the upper and lower bound of the Alfvén continuum (black lines) as function of k_z.

α^n_{mk} and β^n_{mk} are the coefficients of the sine and cosine expansions of the two components of the eigenfunctions respectively.

This approach is described in more detail in Tirry, Berghmans & Goossens (1997) and enables us to obtain an expression which describes the generation of linear MHD waves (coupled fast-Alfvén waves) by radially polarized footpoint motions. Expressions (9) and (10) can be easily evaluated numerically at any time with the structure of the waves fully resolved as long as a sufficiently large numbers of sines in both x and z directions are taken into account.

4. Classification of eigenmodes

When a coronal loop is disturbed, the nature of its response is determined by the spectrum. For $k_y = 0$ and $R = 0$ expression (7) forms two separate eigenvalue problems for the fast and the Alfvén modes. The fast magnetosonic spectrum is governed by

$$\{\rho\omega^2 + \frac{\partial^2}{\partial z^2} + \frac{\partial^2}{\partial x^2}\}\xi_x = 0,$$

whereas the Alfvén spectrum is governed by

$$\{\rho\omega^2 + \frac{\partial^2}{\partial z^2}\}\xi_y = 0.$$

In the latter equation x shows up as a parameter : for each value of x the equation forms a Sturm-Liouville eigenvalue problem. When we vary x, the corresponding discrete spectrum $\{\omega^{(n)}_A(x)\}$ is smeared out in a discrete set of continua. Fig. 1 shows the eigenfrequencies of the first three fast eigenmodes together with the upper and lower bound of the Alfvén continuous spectrum as function of k_z. As seen from the expressions (9) and (10) which describe the solutions as a superposition of eigenmodes, the possible values of k_z are multiples of π/L. The corresponding eigenfrequencies of the fast waves are indicated in Fig. 1 as dots.

In the model of a plasma slab which is inhomogeneous in the x-coordinate and where gravity is ignored, the x-component of the displacement vector ξ_x and the perturbation of total pressure P' are described by the two following equations:

$$\begin{aligned} D\frac{\partial \xi_x}{\partial x} &= -P'(\omega^2 - \omega_I^2)(\omega^2 - \omega_{II}^2), \\ \frac{\partial P'}{\partial x} &= \rho(\omega^2 - \omega_A^2)\xi_x, \end{aligned}$$

where $D = \rho(c^2 + v_A^2)(\omega^2 - \omega_A^2)(\omega^2 - \omega_s^2)$
and where ω_s and ω_A denote the slow and Alfvén frequencies. ω_I and ω_{II} are the cut-off frequencies representing the points where oscillatory behaviour changes to evanescent behaviour or vice versa. In an inhomogeneous medium $\omega_A^2, \omega_s^2, \omega_I^2$ and ω_{II}^2 vary with x and define 4 frequency intervals. For a fixed value of x the following sequence of inequalities is valid:

$$0 \leq \omega_s^2 \leq \omega_I^2 \leq \omega_A^2 \leq \omega_{II}^2.$$

For a pressureless plasma with a uniform magnetic field ($p = 0, B = B_z$), the values of ω_I and ω_{II} are:

$$\omega_I = 0,$$

$$\omega_{II} = \sqrt{k_y^2 + k_z^2}\,\frac{B_z}{\sqrt{\rho}}.$$

The first cut-off frequency ω_I equals zero which leads to the absence of slow waves in our model. Furthermore, for the uncoupled case $k_y = 0$, the second cut-off frequency ω_{II} equals exactly the Alfvén frequency $\omega_A = k_z B_z/\sqrt{\rho}$. Therefore fast modes corresponding to an eigenfrequency above the Alfvén continuum are travelling waves in the exterior coronal environment. In an open system there is a continuous spectrum of these modes above the cut-off frequency ω_{II} and so these 'leaky modes' radiate their energy away from the loop. In our closed box model of a coronal loop they are artificially kept in the neighbourhood of the loop.

The modes with frequency within the range of the continuous spectrum and consequently under the cut-off frequency in the exterior coronal environment, oscillate inside the coronal loop but are evanescent outside the loop. These solutions correspond to what we call the 'body modes' of the loop. For these modes the energy is not radiated away but is stored inside the loop.

For $k_y \neq 0$ the body modes couple to localized Alfvén waves and form essentially quasi-modes (Tirry & Goossens 1996). Due to the resonant coupling, small length scales are generated around the resonant point which enhance dissipation and hence the heating of the loop.

If especially body modes are excited, a lot of energy is stored and is possibly converted into heat through the coupling with the Alfvén modes (i.e. when $k_y \neq 0$). On the other hand, when most of the dominant excited modes are leaky modes, the energy is radiated away in the coronal environment. Thus the nature of the dominant excited modes determines the efficiency of the resonant absorption by Alfvén waves.

However we have some remarks about the coupled case: If we steadily increase the value of k_y from zero, first of all the cut-off frequency ω_{II} no longer equals the Alfvén frequency

but is larger. As a consequence the continuum of leaky modes is shifted upwards.

Secondly the discrete set of body modes will resonantly couple to localized Alfvén continuum modes unless its oscillation frequency shifts out of the Alfvén continuum (see e.g. Tirry & Goossens 1996). Berghmans & Tirry (1997) calculated the continuous change of a quasi-mode frequency with respect to k_y and showed that for relatively small values of k_y, generally the frequency does not move out of the Alfvén continuum. More details about the possible consequences of the coupling will be studied in the related paper by De Groof et al. (1998).

Since the nature of the excited modes in the uncoupled case can only slightly differ from the one in the coupled case, we study in the next section the amount of kinetic energy in both body modes and leaky modes, excited by radially polarized footpoint motions with $k_y = 0$. The ratio of the kinetic energy in the body modes to the kinetic energy in the leaky modes will reveal much information about the efficiency of the resonant absorption in the footpoint driven problem.

5. Kinetic energy in the loop

This section is divided in three subsections. In the first one we derive an analytical expression for the kinetic energy in the coronal loop. Then, in the second subsection, we study the kinetic energy as function of the frequency to analyse the amount of energy in both body and leaky modes. In the third subsection we focus on the kinetic energy of the modes as function of time.

5.1. Kinetic energy contributions

Since the footpoint motions are assumed to be purely radially polarized with $k_y = 0$, only the x-component is excited, so that the total kinetic energy inside the loop is given by

$$E(t) = \frac{1}{2}\int_0^L dz \int_0^b dx\ \rho(x) \left(\frac{\partial \xi_x}{\partial t}\right)^2$$

Since

$$\int_0^L dz \sin\left(\frac{n\pi}{L}z\right) \sin\left(\frac{n'\pi}{L}z\right) = \frac{L}{2}\,\delta_{nn'}$$

and

$$\int_0^b dx\rho(x)\,[|\psi_k^n>_1 |\psi_{k'}^n>_1 + |\psi_k^n>_2 |\psi_{k'}^n>_2] = \delta_{kk'}$$

we can rewrite the expression for the total kinetic energy simply as

$$E(t) = \frac{1}{L}\sum_{n=1}^{\infty}\sum_{k=1}^{\infty} E_k^n(t) \tag{11}$$

where

$$E_k^n(t) = \left(\frac{n\pi}{L}\right)^2 \left(\frac{\partial T_k^n}{\partial t}(t)\right)^2 (\mathcal{R}_k^n)^2.$$

Each term in expression (11) represents the kinetic energy contribution $E_k^n(t)$ of each eigenmode $|\psi_k^n>$.

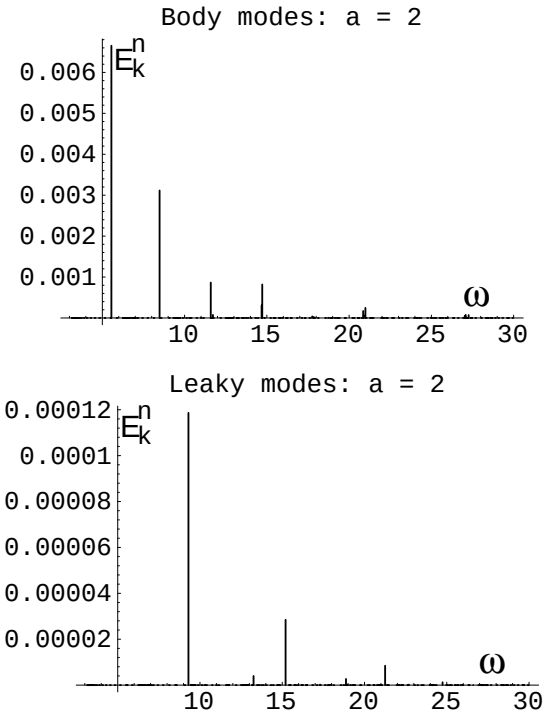

Fig. 2. The kinetic energy averaged in time as function of the frequency for body modes and leaky modes after driving with a pulse of duration π ($a = 2$).

In addition, it is also relevant to look at the contribution of the kinetic energy averaged in time:

$$< E_k^n >= \frac{1}{P}\int_P^{2P} E_k^n(t)dt \tag{12}$$

where P is a period sufficiently longer than any period characteristic to the system or to the footpoint motion.

5.2. Kinetic energy as function of frequency

In this subsection we study how the energy is spread over body and leaky modes.

As an instructive example, rather than a realistic model, we look at a loop with dimensions $L = 1$ and $b = 1$. In this case the characteristics manifest themselves the clearest. The density parameters ρ_A and ρ_B are taken to be 0.6 and 0.4 respectively. In a first approach we want to study the response to footpoint motions with the following time and x dependencies:

$$\begin{aligned} T(t) &= \begin{cases} \sin(at - \frac{\pi}{2}) + 1 & \text{as } 0 \le t \le \frac{2\pi}{a}, \\ 0 & \text{as } t > \frac{2\pi}{a}. \end{cases} \\ R(x) &= \sin(\pi x). \end{aligned} \tag{13}$$

which is chosen in order to simulate an instant 'kick' at the loop's feet.

As the duration of the driving pulse is determined by the value of a, the dominant frequency in the power spectrum of the pulse is given by a. In what follows we look at the kinetic energy distribution for three different values of a.

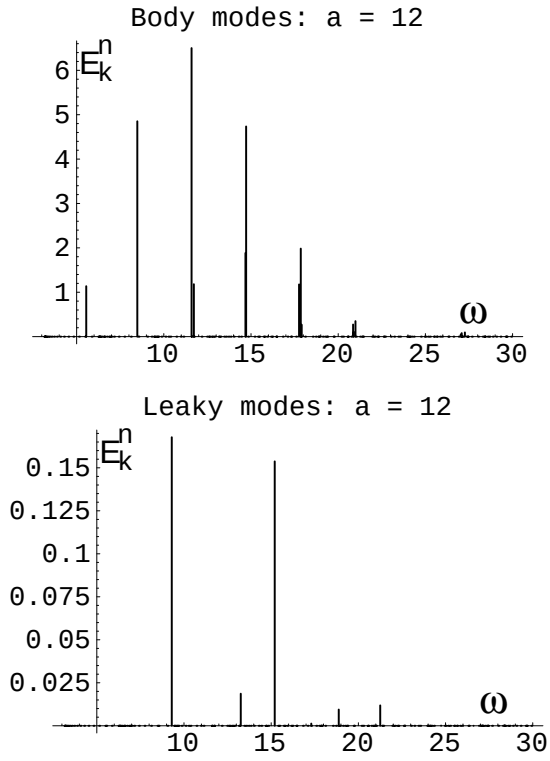

Fig. 3. The kinetic energy averaged in time as function of the frequency for body modes and leaky modes after driving with a pulse of duration $\frac{\pi}{6}$ ($a = 12$).

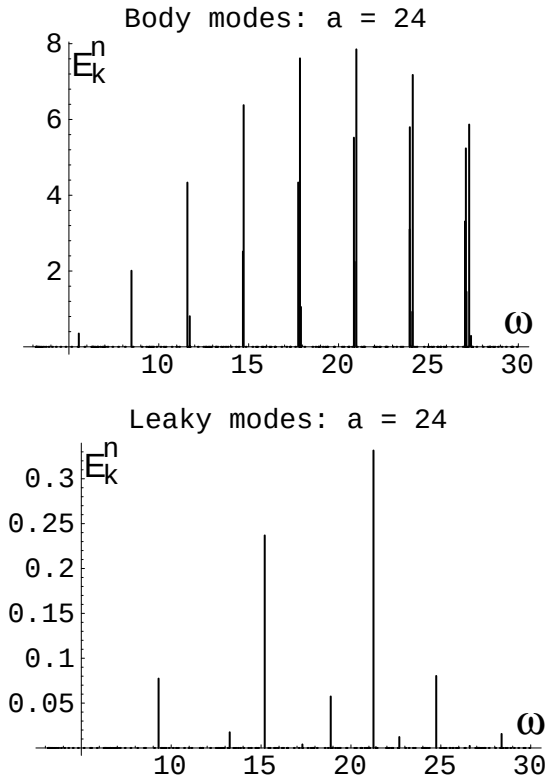

Fig. 4. The kinetic energy averaged in time as function of the frequency for body modes and leaky modes after driving with a pulse of duration $\frac{\pi}{12}$ ($a = 24$).

5.2.1. $\mathbf{a = 2}$

In Fig. 2 we depict the time-averaged kinetic energy contributions (up to a constant factor) of the body modes and leaky modes as a function of the corresponding eigenfrequency. Each spike in these figures corresponds to a dot in Fig. 1 representing a body or leaky mode. As clearly seen, a lot more energy is stored in the excited body modes than in the leaky modes. In consequence, there is more energy stored in the coronal loop than there is radiated away in the coronal environment. In the case where $k_y \neq 0$ such that the body modes couple to the Alfvén waves, this means that a good base is formed for resonant absorption as dissipation mechanism.

As a second point we can remark that predominantly small frequencies are excited. We could have expected this result since the power spectrum of the driving pulse ($\sin(at - \frac{\pi}{2}) + 1$) is dominated by the frequency a=2, which is even smaller than the smallest eigenfrequency $\omega \approx 5.551$.

5.2.2. $\mathbf{a = 12}$

The results corresponding to the driving pulse of duration $\pi/6$ are pictured in Fig. 3. If we compare these figures with Fig. 2, we notice a few differences.

First of all, the total energy in the loop is much larger than in the first case ($a = 2$). The reason is that the dominant frequency in the power spectrum of the pulse is higher and hence more kinetic energy is put into the loop.

Secondly, for the same reason, modes with eigenfrequency around $a = 12$ are most efficiently excited.

Beside these differences, there is also an important similarity. Again most of the energy is stored in the body modes and as a consequence there is not that much energy lost in the coronal environment of the loop.

5.2.3. $\mathbf{a = 24}$

Driving the system with a pulse with $a = 24$ results in Fig. 4. The total kinetic energy again increases and the peak of kinetic energy moves to higher frequencies. Again the by far largest contribution of energy comes from the body modes whereas the leaky modes are almost not excited.

Thus again a good base for resonant absorption as dissipation mechanism is formed.

5.3. Kinetic energy as function of time

To analyse the time evolution of the kinetic energy, we look at two contributions $E_{k,n}$ corresponding to the fundamental body mode ($\omega = 5.551$) and the leaky mode ($\omega = 9.299$) with $k_z = \pi/L$.

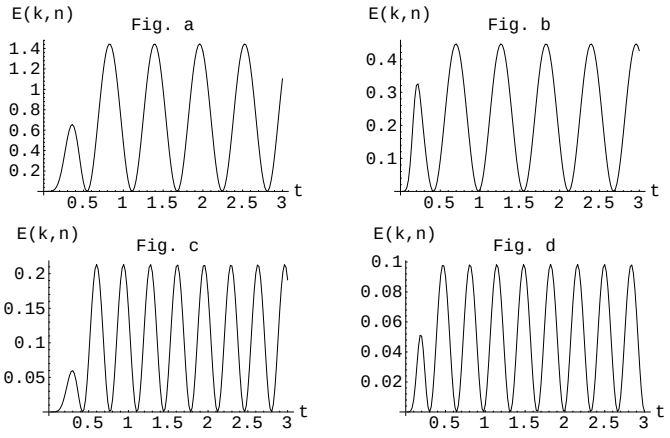

Fig. 5. The time evolution of the kinetic energy for the frequencies $\omega \approx 5.551$ (figures a and b) and $\omega \approx 9.299$ (figures c and d) for $a = 12$ (figures a and c) and $a = 24$ (figures b and d) after one pulse.

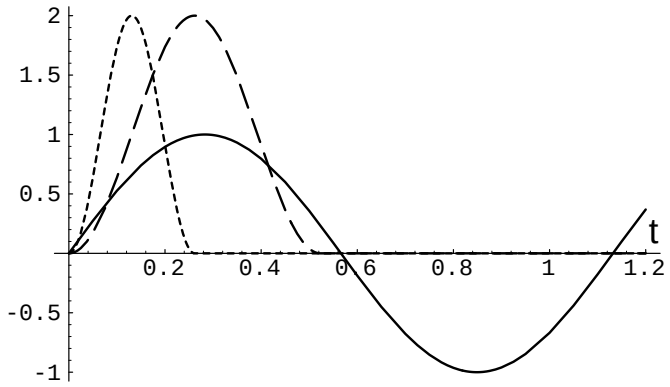

Fig. 6. Comparison of driving pulses with respectively $a = 12$ (dashed line) and $a = 24$ (dotted line) with respect to the eigenfrequency $\omega_k \approx 5.551$ (whole line).

5.3.1. Pulsewise driving

In a first step we again drive the loop with the pulse of the form (13). For the body mode $\omega \approx 5.551$ the time evolution of the energy excited by the driving pulse is plotted on Figs. 5a and 5b respectively for the cases $a = 12$ and $a = 24$.

If $a = 12$ the driving pulse lasts for approximately 0.5 dimensionless time units and after that time there is no more external driving. We notice that after that point the kinetic energy on Fig. 5a shows a regular oscillation. After the driving has stopped the energy of the eigenmode oscillates like $\sin^2(\omega t + \alpha)$ with ω the corresponding eigenfrequency as will be shown later in Sect. 6.

When the driving pulse lasts only for approximately 0.26 time units ($a = 24$), the excited energy is a lot smaller (see Fig. 5b). This is a consequence of the fact that the previous driving pulse, with $a = 12$, approximates the considered eigenoscillation better than the driving pulse with $a = 24$, as one can see in Fig. 6.

Figs. 5c and 5d show the time evolution of the kinetic energy contribution of the leaky mode with $\omega = 9.299$. Just like in the case of the body mode, the kinetic energy is influenced by the

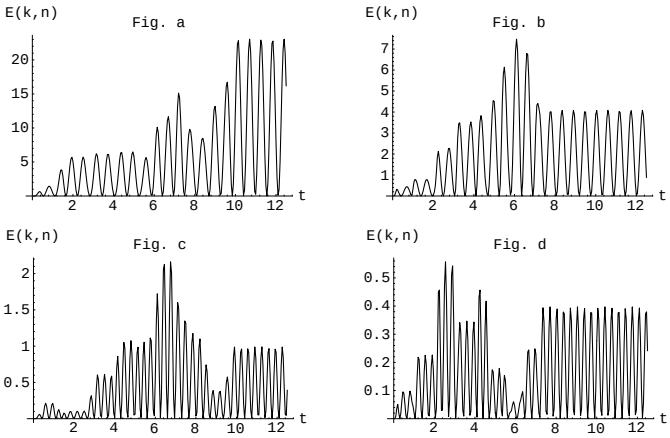

Fig. 7. The time evolution of the kinetic energy for the frequencies $\omega \approx 5.551$ (figures a and b) and $\omega \approx 9.299$ (figures c and d) for $a = 12$ (figures a and c) and $a = 24$ (figures b and d) by driving with 10 identical pulses.

footpoint motion in the beginning and afterwards the energy oscillates like $\sin^2(\omega t + \alpha)$. Note once more that the amount of energy stored in this leaky mode is much smaller than the energy of the body mode.

Finally, as a check, we can compare the time evolution of the kinetic energy (Fig. 5) with the time-averaged kinetic energy as function of the eigenfrequencies (Figs. 3 and 4): the amplitudes of the final oscillations in Fig. 5. are in agreement with the amplitudes of the spikes in Figs. 3 and 4 corresponding to the considered eigenfrequencies.

5.3.2. Stochastic driving

In a next step we drive the system by a succession of identical pulses with random time intervals in between. We take the single pulses equal to the model pulse used in Sect. 5.2.

In what follows we consider a driving with 10 pulses. One can compare this situation with a succession of 10 situations equal to the one in Sect. 5.2. The first pulse generates an oscillation of the eigenmodes. But after the random time interval again the same pulse is given. Dependent on the time in between these two pulses, the second pulse will be in phase or rather out of phase with the generated oscillation. So the amplitude will be increased or decreased respectively under influence of the footpoint motion. In this way each of the 9 subsequent pulses in turn will increase or decrease the kinetic energy. The final result can take various forms. In Fig. 7a to 7d we plotted the time evolution of the kinetic energy contribution corresponding with the frequencies $\omega \approx 5.551$ and $\omega \approx 9.299$ in the cases $a = 12$ and $a = 24$. In a second experiment we used a completely different series of time intervals which resulted in the Fig. 8a to 8d which radically differ from the previous figures. Nevertheless, after the driving has stopped, the kinetic energy again oscillates like $\sin^2(\omega t + \alpha)$ with a constant amplitude. We are interested in the mean value of this final amplitude since it determines the amount of energy which can be stored in the coronal loop (in case of a body mode). By imposing a well defined probability

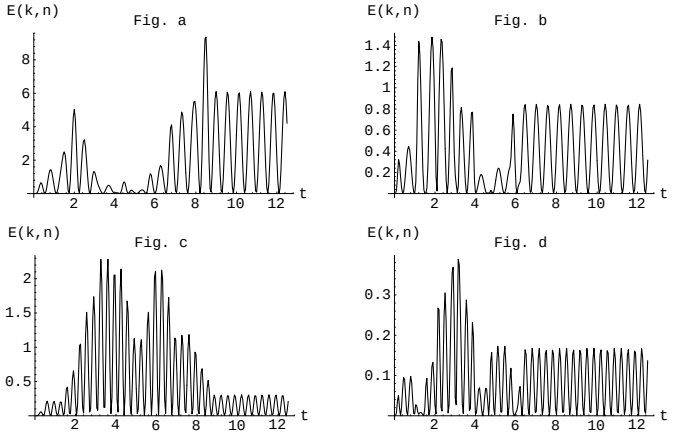

Fig. 8. The time evolution of the kinetic energy for the frequencies $\omega \approx 5.551$ (figures a and b) and $\omega \approx 9.299$ (figures c and d) for $a = 12$ (figures a and c) and $a = 24$ (figures b and d) by driving with 10 identical pulses (second experiment).

distribution function for the time intervals in between the pulses, we analytically derive an expression for the mean value of the final amplitude of the kinetic energy contribution as function of the corresponding frequency and the distribution parameters.

6. Probabilistic description

The aim of this section is to find a relationship between the mean value of the amplitude of the kinetic energy after a stochastic driving with identical pulses and the eigenfrequencies of the loop. To avoid complicated notations we denote the eigenfrequency $\omega_k^{(n)}$ by ω.

We assume the time intervals between the identical pulses to satisfy a well-defined probability distribution. In order to show the effect of the stochastic driving most clearly, we modify the pulse. Instead of the model pulse of the previous section ($\sin(at - \frac{\pi}{2}) + 1$), we now consider pulses with the following time dependence:

$$T(t) = \begin{cases} \sin(at) & \text{as } t_i \leq t \leq t_i + \frac{2\pi}{a}, \\ 0 & \text{elsewhere.} \end{cases}$$

6.1. Energy after $\mathcal{N}$ pulses

In particular we are interested in the single contributions of the eigenfunctions $|\psi_k^n>$ to the total kinetic energy which is represented by Eq. (11) by:

$$E_k^n(t) = \left(\frac{n\pi}{L}\right)^2 \left(\frac{\partial T_k^n}{\partial t}(t)\right)^2 (\mathcal{R}_k^n)^2. \quad (14)$$

The time dependence appears in the second factor $\partial T_k^n/\partial t$. After some algebra we obtain the following result for this time derivative of T_k^n after driving with $\mathcal{N}$ pulses:

$$\begin{aligned} \frac{\partial T_k^n}{\partial t}(t) &= \frac{2a}{\omega^2 - a^2} \sin(\frac{\omega\pi}{a}) \sum_{k=1}^{\mathcal{N}} \sin(\omega t + a_k) \\ &= \frac{2a}{\omega^2 - a^2} \sin(\frac{\omega\pi}{a})\{\cos(\omega t) \sum_{k=1}^{\mathcal{N}} \sin a_k \\ &\quad + \sin(\omega t) \sum_{k=1}^{\mathcal{N}} \cos a_k\} \end{aligned} \quad (15)$$

where $a_k = -\omega[(2k-1)\frac{\pi}{a} + \sum_{j=1}^{k} R_j]$ and $R_1 = 0$.

R_i is the random time interval before the ith pulse.

We can rewrite both summations in expression (15) as follows:

$$\sum_{k=1}^{\mathcal{N}} \sin a_k = A \sin\alpha \qquad \text{and} \qquad \sum_{k=1}^{\mathcal{N}} \cos a_k = A \cos\alpha$$

where

$$A = \sqrt{(\sum_{k=1}^{\mathcal{N}} \cos a_k)^2 + (\sum_{k=1}^{\mathcal{N}} \sin a_k)^2},$$

$$\alpha = \arctan\left(\frac{\sum_{k=1}^{\mathcal{N}} \sin a_k}{\sum_{k=1}^{\mathcal{N}} \cos a_k}\right).$$

Substituting this result in Eqs. (14) and (15), we obtain the following expression for $E_k^n(t)$:

$$E_k^n(t) = \left(\frac{n\pi}{L}\right)^2 (\mathcal{R}_k^n)^2 \frac{4a^2}{(\omega^2 - a^2)^2} \sin^2(\frac{\omega\pi}{a}) A^2 \sin^2(\omega t + \alpha). \quad (16)$$

Hence the final energy oscillates like the square of a sine, with a specific amplitude dependent on the time intervals between the pulses, R_k. As this R_k dependence is included in the factor A^2, in the following subsection we study the influence of the frequency ω on A^2.

6.2. Probabilistic approach

To work out our solution in an analytical way, we assume the intervals between the pulses $R_2, \ldots, R_{\mathcal{N}}$ to satisfy a gamma distribution $\Gamma(\alpha, \beta)$. We are interested in the probability distribution of :

$$\begin{aligned} A^2 &= \left\{\cos\left(\frac{\pi\omega}{a}\right) + \sum_{k=2}^{\mathcal{N}} \cos[\omega((2k-1)\frac{\pi}{a} + \sum_{j=2}^{k} R_j)]\right\}^2 \\ &\quad + \left\{\sin\left(\frac{\pi\omega}{a}\right) + \sum_{k=2}^{\mathcal{N}} \sin[\omega((2k-1)\frac{\pi}{a} + \sum_{j=2}^{k} R_j)]\right\}^2 \end{aligned}$$

or, more specifically, in the mean value of this amplitude.

We solve this problem in four steps:

At first we need the probability distribution function of $S_k \equiv$

$\sum_{j=2}^{k} R_j$. Since $R_j \sim \Gamma(\alpha,\beta)$ for j going from 2 to k and since all R_j are independent, it is easy to check that $S_k \equiv \sum_{j=2}^{k} R_j \sim \Gamma(\alpha(k-1),\beta)$ (Wonnacott & Wonnacott 1990).

As a second step, we calculate the mean value of the first term of A^2. It is convenient to rewrite this 'cosine part' of A^2 as

$$\begin{aligned} EZ_{cos}(\mathcal{N}) &= \cos^2(\frac{\pi\omega}{a}) \\ &+2\cos(\frac{\pi\omega}{a})\sum_{k=2}^{\mathcal{N}} E(\cos[\omega(c_k+S_k)]) \\ &+\sum_{k=2}^{\mathcal{N}}\sum_{l=2}^{\mathcal{N}} E\left\{\cos[\omega(c_k+S_k)]\cos[\omega(c_l+S_l)]\right\}. \quad (17) \end{aligned}$$

Using the definition of mean value and the gamma distribution function, the terms in the first summation can be calculated as $E(\cos[\omega(c_k+S_k)])$

$$= \frac{1}{(1+\omega^2\beta^2)^{\alpha(k-1)/2}}\cos[c_k\omega+\alpha(k-1)\arctan(\omega\beta)]$$

The calculation of the double summation in Eq. (17) is less obvious because $X \equiv S_k \sim \Gamma(\alpha(k-1),\beta)$ and $Y \equiv S_l \sim \Gamma(\alpha(l-1),\beta)$ are two dependent stochastic variables and the mean of a product of two variables only equals the product of the two means if the two variables are independent.

We tackle this problem by rewriting the two successive summations over k and l as a sum of 3 summations where respectively $k>l$, $k<l$ and $k=l$. Since the function

$$E\{\cos[\omega(c_k+S_k)]\cos[\omega(c_l+S_l)]\}$$

is symmetric in k and l, the first two terms in the sum of summations are equal and so we only have to consider the cases $k>l$ and $k=l$.

If $k>l$ we can calculate:

$$\begin{aligned} &E\{\cos[\omega(c_k+S_k)]\cos[\omega(c_l+S_l)]\} \\ &= \frac{1}{2}\int_0^\infty dv\cos[\omega(c_k+c_l+v)]f_{X+Y}(v) \\ &\quad +\frac{1}{2}\int_0^\infty dz\cos[\omega(c_k-c_l+z)]f_{X-Y}(z) \end{aligned}$$

and if $k=l$ we obtain:

$$E\{\cos[\omega(c_k+S_k)]\cos[\omega(c_l+S_l)]\} = E\{\cos^2[\omega(c_k+S_k)]\}.$$

Following the derivation presented in the second step, we rewrite the 'sine part' of A^2. The counterpart of Eq. (17) yields

$$\begin{aligned} EZ_{sin}(\mathcal{N}) &= \sin^2(\frac{\pi\omega}{a}) \\ &+2\sin(\frac{\pi\omega}{a})\sum_{k=2}^{\mathcal{N}} E(\sin[\omega(c_k+S_k)]) \\ &+\sum_{k=2}^{\mathcal{N}}\sum_{l=2}^{\mathcal{N}} E\left\{\sin[\omega(c_k+S_k)]\sin[\omega(c_l+S_l)]\right\} \end{aligned}$$

where

$$E(\sin[\omega(c_k+S_k)]) = \frac{1}{(1+\omega^2\beta^2)^{\alpha(k-1)/2}}\sin[c_k\omega+\alpha(k-1)\arctan(\omega\beta)]$$

and

$$\begin{aligned} &E\{\sin[\omega(c_k+S_k)]\sin[\omega(c_l+S_l)]\} \\ &= \frac{1}{2}\int_0^\infty dz\cos[\omega(c_k-c_l+z)]f_{X-Y}(z) \\ &\quad -\frac{1}{2}\int_0^\infty dv\cos[\omega(c_k+c_l+v)]f_{X+Y}(v), \end{aligned}$$

if $k>l$ and

$$E\{\sin[\omega(c_k+S_k)]\sin[\omega(c_l+S_l)]\} = E\{\sin^2[\omega(c_k+S_k)]\},$$

if $k=l$.

Finally we put the two previous solutions together to find the mean value of A^2 :

$$\begin{aligned} E(A^2) &= 1+2\sum_{k=2}^{\mathcal{N}}\frac{1}{(1+\omega^2\beta^2)^{\alpha(k-1)/2}} \\ &\Big\{\cos(\frac{\pi\omega}{a})\cos[c_k\omega+\alpha(k-1)\arctan(\omega\beta)] \\ &\quad +\sin(\frac{\pi\omega}{a})\cos[c_k\omega-\alpha(k-1)\arctan(\omega\beta)]\Big\} \\ &+2\sum_{l=2}^{\mathcal{N}}\sum_{k=l+1}^{\mathcal{N}}\left\{\int_0^\infty dz\cos[\omega(c_k-c_l+z)]f_{X-Y}(z)\right\} \\ &+(\mathcal{N}-1) \quad (18) \end{aligned}$$

Only the last but one term still has to be worked out. Therefore we need the probability distribution function of $X-Y$. Since in this term k is larger than l we know that $X-Y=\sum_{j=l+1}^{k} R_j$, such that $X-Y \sim \Gamma(\alpha(k-l),\beta)$. So the double summation in Eq. (18) equals

$$\begin{aligned} &2\sum_{l=2}^{\mathcal{N}-1}\sum_{k=l+1}^{\mathcal{N}}\Big\{\frac{1}{(1+\omega^2\beta^2)^{\alpha(k+l)/2}} \\ &\quad\times\cos[(c_k-c_l)\omega+\alpha(k-l)\arctan(\omega\beta)]\Big\} \end{aligned}$$

where $c_i=(2i-1)\pi/a$.

Substituting this result in Eq. (18) we obtain the final result:

$$\begin{aligned} E(A^2) &= \mathcal{N}+2\sum_{k=2}^{\mathcal{N}}\frac{1}{(1+\omega^2\beta^2)^{\alpha(k-1)/2}} \\ &\Big\{\cos(\frac{\pi\omega}{a})\cos[(2k-1)\frac{\pi\omega}{a}+\alpha(k-1)\arctan(\omega\beta)] \\ &\quad +\sin(\frac{\pi\omega}{a})\sin[(2k-1)\frac{\pi\omega}{a}+\alpha(k-1)\arctan(\omega\beta)]\Big\} \\ &+2\sum_{l=2}^{\mathcal{N}-1}\sum_{k=l+1}^{\mathcal{N}}\Big\{\frac{1}{(1+\omega^2\beta^2)^{\alpha(k-l)/2}}\cos[(k-l)\frac{2\pi\omega}{a} \\ &\quad +\alpha(k-l)\arctan(\omega\beta)]\} \end{aligned}$$

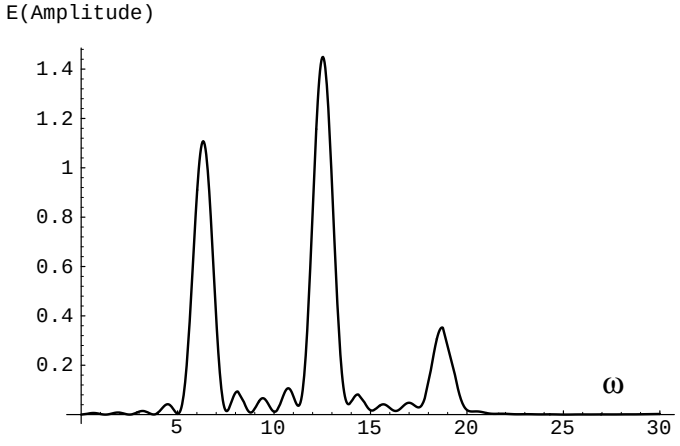

Fig. 9. The mean value of the final amplitude of $\left(\frac{\partial T_k^n}{\partial t}\right)^2$ after driving by a succession of five identical pulses with time intervals in between. These intervals satisfy a gamma distribution with parameters $\alpha = 401$ and $\beta = \frac{1}{800}$.

If we multiply this expression by the factor

$$\frac{4a^2}{(\omega^2 - a^2)^2} \sin^2(\frac{\omega\pi}{a})$$

we obtain, according to Eq. (16), the mean value for the final amplitude of $\left(\frac{\partial T_k^n}{\partial t}\right)^2$ as function of $\omega_k^{(n)}$.

In Fig. 9 we have plotted the mean value of this final amplitude as function of ω for $a = 4\pi$, $\alpha = 401$, $\beta = 1/800$ and $\mathcal{N} = 5$. A gamma distribution with the given parameters α and β is a strongly peaked distribution which is quasi symmetric around the value 0.5. We remark that although this figure shows a continuous graph, the results are only relevant for the discrete eigenfrequencies $\omega_k^{(n)}$. Nevertheless the graph shows remarkable peaks which we try to explain in the next section.

7. Discussion

7.1. Comparison with the power spectrum

Since the gamma distribution function for the time-intervals in between the pulses is strongly peaked around the duration of the pulses, the time dependence of the driving can be approximated by the function

$$f(t) = \sin(at)|_0^{2\pi/a} + \sin(at)|_{4\pi/a}^{6\pi/a} + \ldots + \sin(at)|_{4(\mathcal{N}-1)\pi/a}^{(4\mathcal{N}-2)\pi/a}. \quad (19)$$

The power spectrum of this signal can be easily calculated analytically and is shown in Fig. 10. This figure reflects the remarkable form of the graph in Fig. 9 as was to be expected.

7.2. Comparison with the numerical simulations

As an additional check, we compare the mean value as calculated in Sect. 6.2 with the amplitude of the kinetic energy

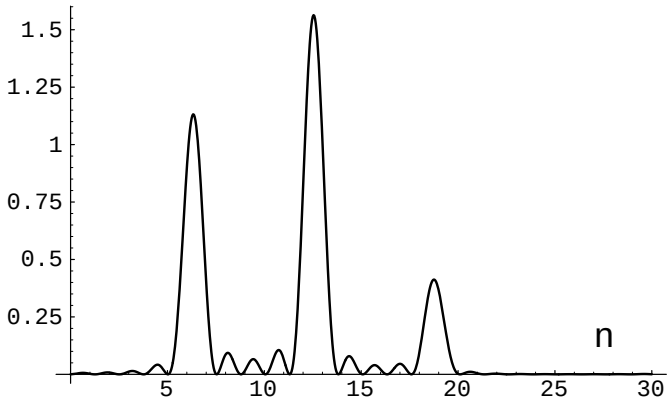

Fig. 10. The power spectrum of the function $f(t)$.

contributions which we obtained numerically after several simulations. We consider the loop to be driven by 5 identical pulses with in between them 40 different series of 4 time intervals each satisfying a $\Gamma(401, \frac{1}{800})$ distribution. After each simulation we look for the final amplitude of $\left(\frac{\partial T_k^n}{\partial t}\right)^2$ for three different eigenfrequencies, namely $\omega_k^{(n)} \approx 5.551$, $\omega_k^{(n)} \approx 9.299$ and $\omega_k^{(n)} \approx 13.256$.

$\omega_{\mathbf{k}}^{(\mathbf{n})} \approx \mathbf{5.551}$

The probabilistic calculations we did in the previous section predict $\left(\frac{\partial T_k^n}{\partial t}\right)^2$ to oscillate with an average amplitude of approximately 0.286 (see Fig. 9).

In our numerical solutions we found for the final amplitude 40 different values which all lie between 0.22 and 0.37 with an average value around 0.27. The standard deviation

$$\sigma = \sqrt{\frac{\sum_{i=1}^{40}(x_i - \bar{x})^2}{40}}$$

is 0.051. Thus our first check is very satisfying since the values we found all approximate the predicted average.

$\omega_{\mathbf{k}}^{(\mathbf{n})} \approx \mathbf{9.299}$

For this eigenfrequency of the coronal loop the calculations predict an average amplitude of 0.0616. We again did similar numerical simulations and we found 40 values lying between 0.045 and 0.072. The average of the values now equals approximately 0.060 and the standard deviation equals 0.0089. These results again seem to show that our probabilistic calculations are relevant.

$\omega_{\mathbf{k}}^{(\mathbf{n})} \approx \mathbf{13.256}$

The predicted value for the amplitude is 0.489 and this value is closely approximated by the different results of the numerical code as it should be. This time the standard deviation is

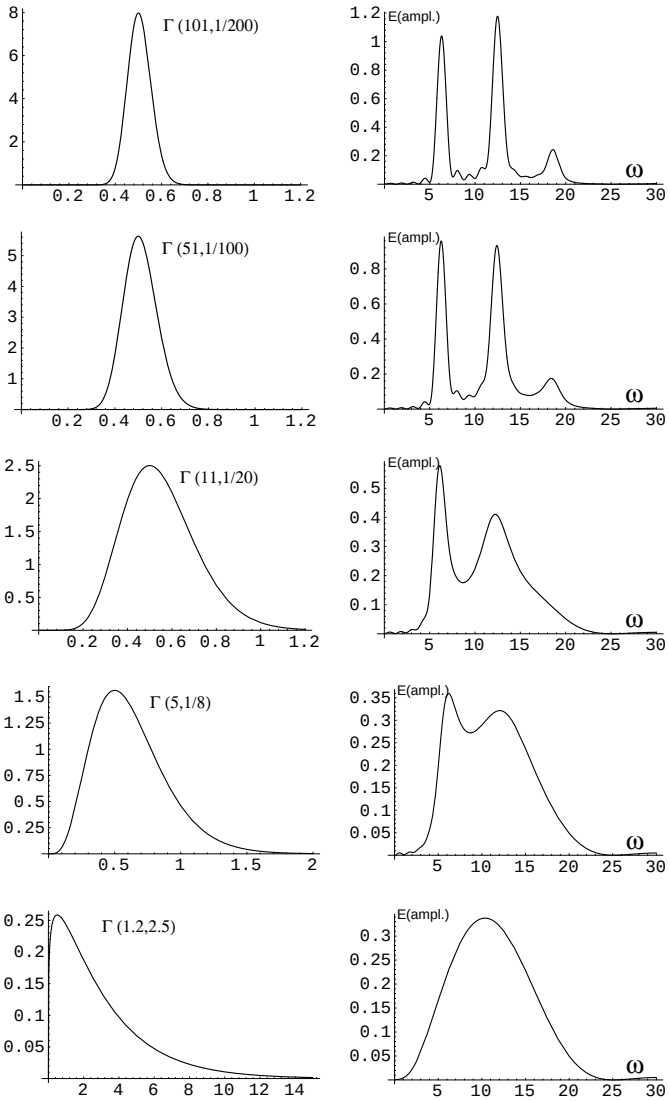

Fig. 11. Five gamma distributions together with the corresponding graphs for the average of the final amplitude of $\left(\frac{\partial T_k}{\partial t}\right)^2$ after driving the loop with five identical pulses with a frequency $a = 4\pi$.

larger, namely 0.20, but the average, in this case 0.52, again approximates the predicted value.

7.3. Influence of the gamma distribution

As mentioned before Figs. 9 and 10 are very similar because of the strongly peaked gamma distribution. Now we are interested to see how Fig. 9 changes if we consider a less peaked gamma distribution.

Fig. 11 shows five less peaked gamma distributions with mode 0.5 on the left hand side and on the right hand side the corresponding graphs for the average of the final amplitude of $\left(\frac{\partial T_k^n}{\partial t}\right)^2$ after driving by five pulses characterized by $a = 4\pi$. As expected the fine structure in the variation of the mean value of the amplitude with respect to ω disappears and the amplitude of the peaks decreases as the gamma distribution becomes wider and hence as the time intervals between the pulses vary more. The two outer dominant peaks of Fig. 9 first remain but they disappear as the gamma distribution widens. In addition we notice that the large contrasts in the figure seem to weaken first for large frequencies and only later on for the small frequencies. In the end, for gamma distributions with small parameter α, the graph is reduced to one wide peak around $\omega = a$, as shown on Fig. 11 in the case of $\Gamma(1.2, 2.5)$.

8. Summary

In this paper we studied the excitation of fast MHD waves in a coronal loop driven by radially polarized footpoint motions. The main topic was to extend previous analyses, in which the driving was assumed to be harmonic, to a stochastic driving. As a first step we assumed the loop to be driven by a train of identical pulses with random time intervals in between. The solution is written as a superposition of eigenmodes, which can be classified to be either 'leaky' or 'body' modes. The leaky modes radiate their energy away from the loop, whereas the body modes, which are trapped in the loop cavity, may resonantly couple to Alfvén waves and in this way dissipate their energy.

Firstly, by analysing the response to a kick at the loop's feet, we found that most of the input energy is stored in the body modes. Hence driving at the loop's feet forms a good base for resonant absorption as heating mechanism.

Secondly, by imposing the time intervals between the pulses to satisfy a gamma distribution, we analytically derived a relation between the mean value of the kinetic energy contribution of each eigenmode and the corresponding eigenfrequency. The remarkable peaked structure, obtained in the case of a very peaked gamma distribution, reflects very well the power spectrum of the footpoint driving.

Also the output of the several numerical simulations were in agreement with the predicted analytical result for the final amplitude after the driving with a train of pulses.

By considering gamma distributions with greater variance, we showed how the peak structure disappears in the variation of the mean value as function of the frequency. In order to determine the efficiency of resonant absorption in case of this stochastic driving at the loop's feet, it is very important to know where the eigenfrequencies of the body modes are located in comparison with the peaks in a figure like Fig. 9. Hence parametric studies for loops with different 'realistic' dimensions with 'realistic' parameters for the gamma distribution (and others) should be done. On the other hand, it is also important to find out how efficient the energy is transferred from the body modes to the resonant Alfvén waves under the stochastic footpoint driving. This implies to study the case with $k_y \neq 0$ which is the main topic of De Groof et al. (1998).

References

Berghmans, D., De Bruyne, P. 1995, ApJ, 453, 495
Berghmans, D., De Bruyne, P., Goossens, M. 1996, ApJ, 472, 398
Berghmans, D., Tirry, W.J. 1997, A&A, 325, 318

Chen, L., Hasegawa, A. 1974, Phys. Fluids, 74, 1399
De Groof, A., et al. 1998, in preparation
Goedbloed, J.P., Halberstadt, G. 1994, A&A, 286, 275
Gomez, D. 1990, Fund. Cosmic Phys., 14, 131
Goossens, M., 1991, in E.R.Priest and A.W.Hood (eds.), 'MHD Waves and Wave Heating in Non-Uniform Plasmas', *Advances in Solar System Magnetohydrodynamics*, Cambridge University Press, Cambridge, p. 135.
Halberstadt, G., Goedbloed, J.P. 1995, A&A, 301, 559
Heyvaerts, J., Priest, E.R. 1983, A&A, 117, 220
Hollweg, J.V. 1984, ApJ, 277, 392
Ionson, J.A. 1978, ApJ, 226, 650
Kappraff, J.M., Tataronis, J.A. 1977, J.Plasma Phys., 18, 209
Ofman, L., Davila, J.M. 1995, J. Geophys. Res., 100, 23427
Ofman, L., Davila, J.M. 1996, ApJ, 456, L123
Parker, E.N. 1972, ApJ, 174, 499
Poedts, S., Goossens, M., Kerner, W. 1989, SPh, 123, 83
Poedts, S., Kerner, W. 1992, J. Plasma Phys., 47(1), 139
Ruderman, M.S., Berghmans, D., Goossens, M., Poedts, S. 1997, A&A, 320, 305
Steinolfson, R.S., Davila, J.M. 1993, ApJ, 415, 354
Strauss, H.R., Lawson, W.S. 1989, ApJ, 346, 1035
Tataronis, J.A., Grossmann, W. 1975, J. Plasma Physics, 13, 87
Tirry, W.J., Goossens, M. 1996, ApJ, 471, 501
Tirry, W.J., Berghmans, D., Goossens, M. 1997, A&A, 322, 329
Tirry, W.J., Berghmans, D. 1997, A&A, 325, 329
Wonnacott, T.H., Wonnacott, R.J. 1990, *Introductory Statistics*, fifth edition, John Wiley & Sons
Wright, A.N., Rickard, G.J. 1995, ApJ, 444, 458